



Microwave Sensing for Avoidance of High-Risk Ground Conditions for Mobile Robots

DOI:

[10.1109/COINS57856.2023.10189266](https://doi.org/10.1109/COINS57856.2023.10189266)

Document Version

Accepted author manuscript

[Link to publication record in Manchester Research Explorer](#)

Citation for published version (APA):

Blanche, J., Mitchell, D., West, A., Harper, S., Groves, K., Lennox, B., Watson, S., & Flynn, D. (2023). Microwave Sensing for Avoidance of High-Risk Ground Conditions for Mobile Robots. In *IEEE International Conference on Omni-Layer Intelligent Systems (COINS) 2023* IEEE. Advance online publication. <https://doi.org/10.1109/COINS57856.2023.10189266>

Published in:

IEEE International Conference on Omni-Layer Intelligent Systems (COINS) 2023

Citing this paper

Please note that where the full-text provided on Manchester Research Explorer is the Author Accepted Manuscript or Proof version this may differ from the final Published version. If citing, it is advised that you check and use the publisher's definitive version.

General rights

Copyright and moral rights for the publications made accessible in the Research Explorer are retained by the authors and/or other copyright owners and it is a condition of accessing publications that users recognise and abide by the legal requirements associated with these rights.

Takedown policy

If you believe that this document breaches copyright please refer to the University of Manchester's Takedown Procedures [<http://man.ac.uk/04Y6Bo>] or contact uml.scholarlycommunications@manchester.ac.uk providing relevant details, so we can investigate your claim.



Millimeter-Wave Sensing for Avoidance of High-Risk Ground Conditions for Mobile Robots

IMPORTANT: All regular papers go through a blind peer-review process. Therefore, your submission must not include information that serves to identify the authors of the manuscript, such as name(s) or affiliation(s) of the author(s), anywhere in the manuscript, abstract, or in the embedded PDF data. References and bibliographic citations to the author(s) own published works or affiliations should be made in the third person.

Abstract—*To be useful in a wider range of environments, especially environments that are not sanitized for their use, robots must be able to handle uncertainty in ground conditions. This requires a robot to incorporate new sensors and sources of information, and to be able to use this information to make decisions regarding navigation. When using autonomous mobile robots in unstructured and poorly defined environments ground condition is of critical importance and is a common cause of failure, an example being the presence of ground water in the operating area. To evaluate a non-contact sensing method to mitigate this risk, Frequency Modulated Continuous Wave (FMCW) radar is integrated with an Unmanned Ground Vehicle (UGV), representing a novel application of FMCW to detect new measurands for Robotic Autonomous Systems (RAS) navigation, informing on ground integrity and adding to the state-of-the-art in sensing for optimized autonomous path planning. In this paper, FMCW is first evaluated in a desktop setting to determine water sensing capability. The FMCW is then fixed to a UGV, and the sensor system is successfully tested and validated in a representative environment containing regions with significant levels of ground water saturation.*

Keywords - Path Planning, Robotics in Hazardous Fields, Robot Safety.

I. INTRODUCTION

The use of robotics in the industrial and commercial sectors is well established, with facilities increasingly designed around the needs of a robotic fleet [1]. The predictable and managed operating conditions within such facilities are optimized towards the efficient operation of wheeled robotic agents, for example smooth concrete flooring in warehouses, as typified in Figure 1. However, the practical application of robotic systems in unmanaged dynamic environments require runtime path planning capable of identifying a safe route for navigation through areas less suitable for robotic operations [2]. Accounting for environmental dynamism in path planning for Robotic Autonomous Systems (RAS), while an established field, places a focus on object detection and collision avoidance as

part mobile Simultaneous Location And Mapping (SLAM) operations [3]. However, less research emphasis is placed on ground condition and ground integrity monitoring as a means of determining a route of safe passage through an area of uncertain ground integrity that may otherwise impede the RAS. In a warehouse environment, such ground integrity contrasts could be typified as fluid spillage on smooth concrete, representing compromised traction for a loaded wheeled robotic agent and a significant threat to autonomous control. An alternate use case is the detection and tracking of hazardous spills in chemical or nuclear storage facilities.

The state-of-the-art in edge dynamic path planning has resulted in autonomous mobile robots that can account for uncertainty in the conditions of its operational environment, with navigational decisions made based on information from a suite of sensors [4]. Costmaps, gridded map representations of risk used in 2D path planning and navigation, can provide semi-autonomous systems with awareness of the position of static and mobile obstacles in an environment using sensors, such as lidar or depth cameras [5]. Path planning algorithms then use this information to avoid areas where a collision may occur [6]. This costmap approach provides robots with a spatially resolved representation of risk, which can be expanded to a range of sensing modalities and threats. An example is the integration of ionizing radiation sensing with Unmanned Ground Vehicles (UGVs) to map radiation levels in deployment areas where human presence is denied due to the radioactive environment [7]. This places greater emphasis on edge sensing to both detect and map high risk areas, in addition to safeguarding the robotic platform by preventing a condition of irretrievable failure. The consequent evasion of highly localized radiation levels improves mission resilience and advances the RAS capacity for non-intervention in a hazardous environment.

The detection of water and other fluids, such as oil or lubricants, on surfaces via robotics represents a major factor in autonomous mission viability, where a loss of traction may result in the loss of the platform when operating in a human-denied environment. To date, research coupling fluid detection and robotic platforms is limited to sensors that require physical contact with the ground, such as force/torque sensors coupled with inertial measurement units and joint encoders [8]–[12].

IMPORTANT: All regular papers go through a blind peer-review process. Therefore, your submission must not include information that serves to identify the authors of the manuscript, such as name(s) or affiliation(s) of the author(s), anywhere in the manuscript, abstract, or in the embedded PDF data. References and bibliographic citations to the author(s) own published works or affiliations should be made in the third person.

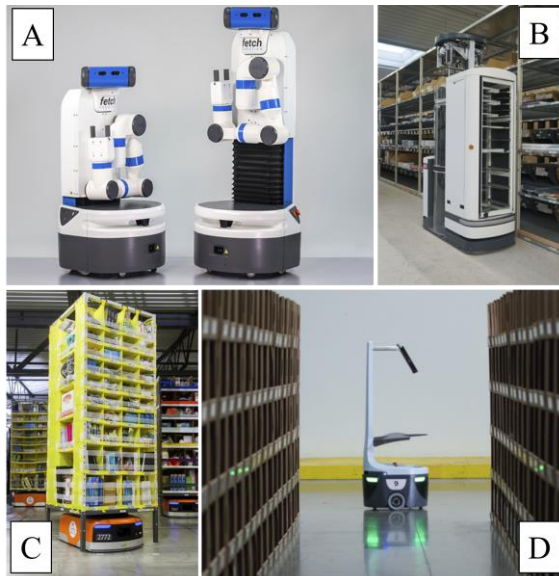


Figure 1. Wheeled robotic platforms designed for use in warehouse environments. A) Fetch, B) Magazino GmbH, C) Amazon, D) Locus [13]

This is far from ideal as the robotic platform, in acquiring data, must commit to being present, and exerting force, at the site of uncertainty and the risks associated with that site. To maintain an appropriate standoff capability, in the order of centimeters/meters, a non-contact method of sensing is needed. This may be of particular importance in situations where contaminants may be transported by the RAS coming into contact with water.

One method of non-contact sensing that has seen use on RAS is Frequency Modulated Continuous Wave Radar (FMCW) radar, a low-power, non-contact method of detecting the presence of obstacles to aid the calculation of effective paths through a cluttered area. This modality is also used for Speed and Separation Monitoring (SSM) of moving targets, with the key measurands being the time of flight (distance) and doppler shift (relative speed) [14]–[19]. This method has been favored for use in hazardous and extreme environments due to being unaffected by ambient lighting, fog, mist and smoke, making FMCW a strong candidate technology to augment orthodox SLAM technologies, such as LiDAR, in conditions where optical methods fail. A summary of the above publications is given in Table 1, where the sensor types and measurands, in addition to the RAS platforms utilized are shown. The key observations of this literature review are that ground condition monitoring is limited to sensors that require physical contact with the surface being assessed. Additionally, the use of FMCW radar on RAS to date has been to augment obstacle detection and dynamic target tracking for SLAM in conditions where optical sensors may be inhibited and has not been used to determine ground condition for RAS operations.

FMCW ground integrity sensing in the X- and K-bands has been successfully applied to the detection of contrasts in layered low to medium dielectric media, such as snow and ice stratigraphy, with sensors deployed on hauled sleds to generate a stratigraphic image of the snow subsurface [20]–[24]. In the K-band, FMCW has been found to be effective

for contrast detection in soils [25], [26], fluid presence in sandstones, sands and concretes [27], in addition to the detection of failure precursors in loaded sandstones [28]. FMCW is an emergent sensing modality in many other sectors, such as medical monitoring [29], [30], automotive [31]–[35], aerospace [36]–[38], security and surveillance [39]–[41], energy sector asset integrity [42], [43].

A key enabler towards the robotic deployment of the above sensor modes includes the integration with RAS to inform their decision making and controlling algorithms [44], at the agent scale, while also providing condition parameters of the operating environment. As such, this research represents the novel fusion of emergent sensor modes with the state-of-the-art in autonomous dynamic path planning for robotic agents required to operate in hazardous or Beyond Visual Line Of Sight (BVLOS) conditions. The successful integration of FMCW radar with autonomous environmental characterization and mapping has the potential to provide new measurands of terrain integrity data, such as the detection of water, snow, ice, oil or other contaminants on the operating surface that may otherwise inhibit the operation/motion of a UGV. FMCW can also provide subsurface data if the surface is of low to medium dielectric strength. Providing robotic systems with situational awareness of ground integrity via FMCW sensing allows these systems to autonomously avoid associated hidden or previously undetectable navigation risks, therefore increasing their operational lifetime and reducing the need for intervention. Understanding the subsurface in real world operating environments will require consistent detection of contrasts and instabilities in stratigraphic layers, where the passage of a robot would have a high likelihood of slippage or stranding. This also translates into the potential for hidden object or void detection in snow, sand, soil, ice and some rock types.

This paper presents the benchmarking and testing of a K-band FMCW sensor system to detect surface moisture and standing water on concrete, representing an analogue of a warehouse floor robotic operating area. For clarity, the FMCW is not being used as a time of flight or doppler shift sensor in this application. With a known distance to the target, the key information comes from contrasts in the return signal amplitude and phase, which can be used to infer ground condition via the detection of known thresholds for fluid presence. The addition of moisture and standing water is representative of an operating hazard in an area optimized for robotic operations; and where the presence of water and transported contaminants is damaging to robot systems and a threat to traction for loaded autonomous ground vehicles. For example, this may be due to cargo spillage or warehouse roof failure, in an industrial context, or due to structural degradation in areas denied to human access, for example areas sealed off due to radiation and leaks in legacy waste storage sites.

The remainder of this paper is structured as follows; Section II presents the FMCW theory and section III provides the operating parameters and outlines FMCW operation. Section IV presents the experimental tests and results. Section IV.A presents static testing, where the FMCW sensor is held above

TABLE 1 Summary of sensors used for assessment of traction, inferring ground integrity (upper) and summary of sensors used for SLAM (lower).

Robots sensing ground conditions					
Method	Contact?	Measurement/Measurand	Platform	Critique	Ref
Biomimetic FMSS (load)	Yes	Load/friction coefficient(slip)	Bipedal	Requires physical contact with surface to assess condition	[9]
F/T sensors					[10]
IMU, F/T, joint encoders			Quadruped		[8]
FMCW for robot sensing					
Use	Antenna Type	Frequency Band	Platform	Critique	Ref
Obstacle SLAM	Rotating Monostatic	K (24.125GHz)	Autonomous Vehicle	Used as augmentation for "standard" SLAM and not for ground integrity	[14], [15]
	Fixed MIMO	Ku (16-18 GHz)			[16]
	Monostatic Patch	K (24 GHz)	UAV		[17]
SSM		60 GHz	Robot arm		[18]
	Bistatic Patch	120 -150 GHz	Industrial Robotics		[19]

a concrete test area to give an unchanging field of view. This is to establish baselines and contrasts under simple operating conditions. Section IV.B presents dynamic testing, where the FMCW is mounted on a Clearpath Husky A200 UGV, via a Universal Robotics UR5 manipulator arm, and concrete is scanned during transit of the robot over the test area. This is to evaluate the stability of the signal and suitability for integration with thresholding algorithms and subsequent use in a costmap for terrain mapping and autonomous path planning. Section V discusses the acquired data and section VI concludes.

II. FMCW THEORY

Represented by a continuous wave sweep of the bandwidth, the output of the FMCW sensor is modulated to create a saw-tooth waveform. The difference in frequency between the emitted and return signals is determined by summing output and input waveforms to give a low frequency signal, which is then analyzed to infer the properties of an object in the Field Of View (FOV). This is termed the intermediate frequency (IF) signal of frequency Δf , as shown in Figure 2. The determination of the IF signal is as follows [45]:

$$f_{RF_{out}} = f_{RF_0} + k_f \times t \quad (1)$$

where $0 \leq t \leq T$, f_{RF_0} is the starting frequency, T is the frequency sweep and k_f is the sweep rate.

$$k_f = \frac{B}{T} \quad (2)$$

where B is the sweep bandwidth and the two-way time (TWT) of the emitted signal calculated as:

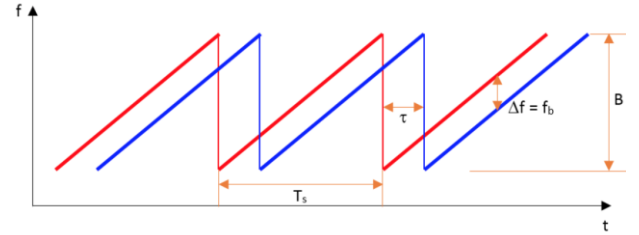


Figure 2 "Sawtooth" Transmitted and Received signals from the FMCW module, where f = frequency, t = time, T_s = sweep duration, τ = two-way travel time of return signal, B = sweep bandwidth and Δf = intermediate frequency.

$$\tau = 2 \frac{d}{c} \quad (3)$$

where d is the distance between the antenna and the reflecting target and c is the speed of light in air. Therefore, due to the observed delay in return signal, the return frequency compared to the emitted frequency will be:

$$f_{R_{received}} = f_{RF_0} + k_f \times (t - \tau) \quad (4)$$

where, $\tau \leq t \leq T + \tau$.

The difference in frequency (Δf), or IF, between the emitted and received signal is therefore:

$$\Delta f = k_f \times (-\Delta t) \quad (5)$$

The negative time of flight can be taken as a magnitude, allowing for the expression:

$$\Delta f = \frac{B}{T} \times 2 \frac{d}{c} \quad (6)$$

Due to the relationship expressed in equation (6), the distance between the sensor and target is kept constant. Thereby, any

signal variation can be attributed to the target surface intrinsic properties, as long as d is known.

FMCW operating in normal mode (perpendicular to target) represents a non-contact means for target property analysis. Consequently, this section outlines the reflection coefficient value for microwave radiation transmitted through a planar interface of refractive index η_2 [46]

The reflection coefficient, Γ , quantifies the fraction of incident radiation intensity reflected at a planar interface, where E_{incident} is the amplitude of the incident wave and $E_{\text{reflected}}$ is the amplitude of the reflected wave, as shown in (7). Assuming a normal, planar incident wave in air with refractive index η_1 , the reflected wave in a medium with refractive index η_2 may be described,

$$|\Gamma| = \frac{E_{\text{reflected}}}{E_{\text{incident}}} = \frac{\eta_1 - \eta_2}{\eta_1 + \eta_2} \quad (7)$$

where an increase in η_2 corresponds to an increase in Return Signal Amplitude (RSA) due to the relationship between refractive index, η , and relative permittivity, ϵ_r (8), and where the relative permittivity of water (~ 80) is significantly higher than that of dry concrete (3.5~7.8) [47]–[49].

$$\epsilon_r = \eta^2 \quad (8)$$

III. EQUIPMENT SETUP AND OPERATING PARAMETERS

Using a direct SMA/SMA coupling (rated to 26 GHz), the K-band radar module was connected to a Flann 21-240 Standard Gain Horn (SGH) antenna. The key operating parameters are shown in Table 2 [50], [51]. Figure 3 provides a block diagram of the sensor setup and analytical workflow. Evaluation of the utilized Flann Microwave antenna shows it to have a peak amplitude spot size on the target of ~ 36.4 millimeters radius at an antenna – target separation of 10 cm. Assuming a consistent near field divergence of 15° (Figure 4A) for the radiation pattern emitted from this antenna, the FOV for a target separation of 30 cm is $\sim 20 \times 10^{-3} \text{ m}^2$. Within this FOV, a minimal phase differential is observed (Figure 4B) [50], [51].

IV. EXPERIMENTAL TESTS AND RESULTS

A. Static Testing

To evaluate the sensitivity of a statically-mounted FMCW sensor to moisture on smooth concrete, two experiments were conducted. Experiment A used an area of dry concrete as a baseline, prior to the passing of a wet cloth over the test area after a period of 10 seconds (Figure 5A). Experiment B repeated Experiment A with the deposition of ~ 20 milliliters of water in the sensor FOV after ~ 10 seconds (Figure 5B). Figure 6 shows the amplitude response of the FMCW sensor for each contrast agent condition within the test area. Clear contrasts are observed for both applied moisture conditions, experiments A and B, with a correlation between volume of water present and amplitude response. The same correlation is seen in Figure 7, which shows the phase shift response of the FMCW sensor, and where an increase in water volume in the sensor FOV corresponds to an increasingly negative shift in the return signal phase.

B. Dynamic Testing: Motion on an Autonomous Vehicle

The Clearpath Husky A200 UGV-mounted FMCW can be seen in Figure 8, where the antenna is protected within a low dielectric PolyLactic Acid (PLA) enclosure to allow a gripping point for the UR5 manipulator. The tip of the antenna is 30 cm from the concrete surface. The extent of the test area is indicated by the blue overlay and is bounded by tape markers on the concrete floor. The FOV of the sensor, indicated by the orange and yellow cone overlay, traverses an area where moisture was applied as a contrast agent and that is flanked by regions of dry concrete within the test area. Data was acquired under three surface moisture conditions:

1. A “dry” control scan, where the robot advances slowly over the test area, which was not wetted. This dataset acts as a baseline.
2. A “damp” scan, using the same test area boundaries and rate of transit as before, but with the midpoint of the test area dampened with a wet cloth.
3. A “wet” scan with the same test area saturated with ~ 100 ml of water.

TABLE 2. FMCW PARAMETERS FOR STATIC AND DYNAMIC TRIALS

Parameter	Value
Band	K- Band (24 – 25.5 GHz) Bandwidth 1500 MHz
Chirp Duration	300 milliseconds
Field Of View on Target (30 cm)	$20 \times 10^{-3} \text{ m}^2$
Intermediate Frequency of Target (30 cm)	12 MHz (or 24.012 GHz)
Sample Rate	0.5 Hz
Data Transmit Time	1.2 seconds
Analysis Time	31 milliseconds

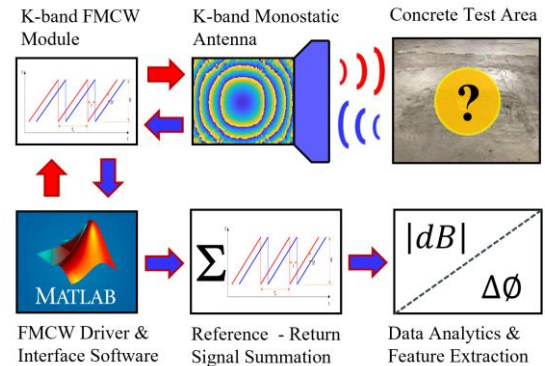


Figure 3. Block diagram of the sensor setup and analytical workflow, where the red (clockwise) arrows indicate the transmitted signal stages and the blue (counter-clockwise) arrows represent the received signal and data processing stages.

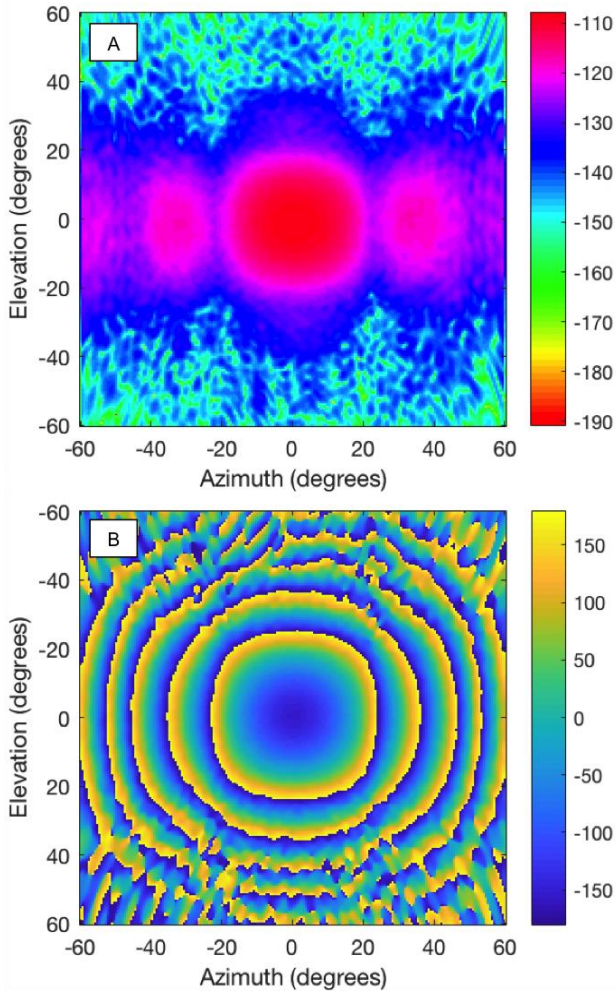


Figure 4. Emission characterization detail for K-Band Flann Microwave antenna model 21240-20. All data taken on a plane at 10 cm antenna – probe separation. A) Amplitude (scale bar in dBm) and B) Phase Shift (scale bar in degrees) [51].



Figure 5. A) A wet cloth was applied to dampen the test area, note light surface sheen due to moisture. B) ~20 ml of water deposited in the sensor field of view.

In each instance, the movement of the Husky A200 is from point 1 to point 2, as indicated in Figure 8. Figure 9 shows the RSA response at an Intermediate Frequency (IF) of 12 MHz for the three surface moisture conditions. This IF corresponds to a 30 cm height from the ground to the sensor tip. The legend in Figure 9 describes the sequence of target conditions, with each start and end point being dry. A key observation of these datasets shows, as in the static data, there is a direct relationship between RSA and water volume in the sensor FOV. The relationship between the surface moisture conditions for the return signal phase can be seen in Figure 10, where clear responses are evident.

V. DISCUSSION

Static testing shows that the RSA is sensitive to the volume of water in the sensor FOV, with observed consistency between the dry concrete baseline and increasing degrees of water presence. This same consistency is also observed in the phase shift, with a higher degree of water in the sensor FOV resulting in a higher phase shift from a common initial condition. These tests validate the suitability of the FMCW sensor as a fixed position sensor to inform on

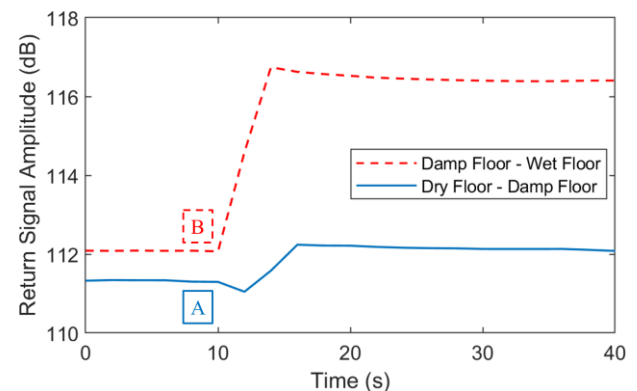


Figure 6. Static FMCW return signal amplitude over time for the intermediate frequency corresponding to the concrete floor interface at 12 MHz within the frequency sweep (or 24.012 GHz). A) Experiment A and B) Experiment B.

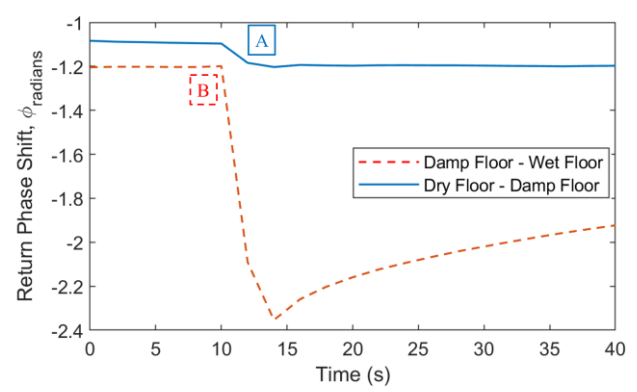


Figure 7. Static FMCW return phase shift over time for the intermediate frequency corresponding to the concrete floor interface at 12 MHz. A) Experiment A and B) Experiment B.

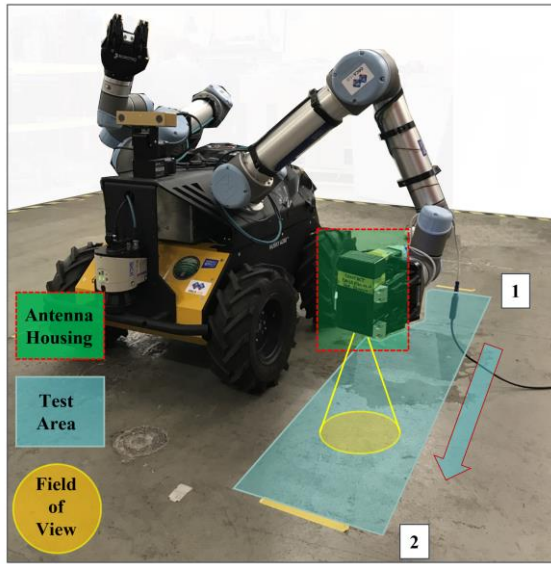


Figure 8. Experimental setup and cartoon overlay of test area and sensor field of view. Sensor tip is at a height of 30 cm above ground level. Points 1 and 2 indicate the direction of travel for each data acquisition.

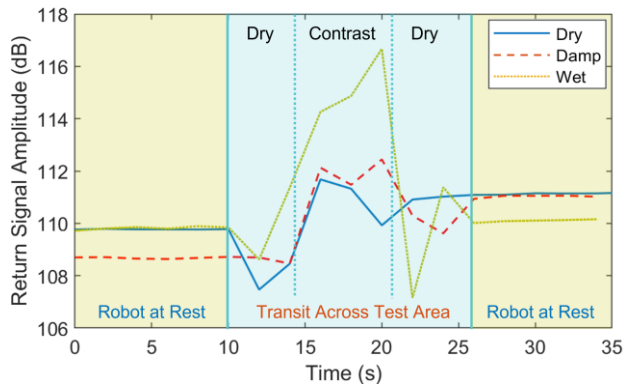


Figure 9. Dynamic FMCW return amplitude over time for the intermediate frequency corresponding to the concrete floor interface at 12 MHz.

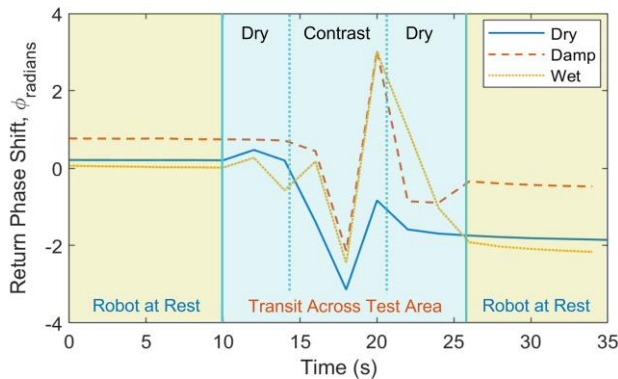


Figure 10. Dynamic FMCW return phase shift over time for the intermediate frequency corresponding to the concrete floor interface at 12 MHz.

ground condition contrasts within a single FOV. Dynamic testing shows clear signal contrasts in varying surface moisture condition scenarios for both amplitude and phase responses. The relationships observed in the static testing phase are consistent with the dynamic data acquired, however, this phase of testing has identified the need to adapt the sensing parameters to improve the rate of data acquisition and signal variance. The advantages of an increased rate of data acquisition are twofold: to allow data averaging and thresholding algorithms, such as applied in [6] and [7], to update a costmap closer to real time. Higher data acquisition rates also allow for faster UGV transit through the test area.

As discussed in [6], the sampling rate must be of sufficient frequency that the UGV can update its costmap, plan new paths to avoid areas of undesirable ground integrity, and the robot begins execution of the new path, all prior to committing to traversing an undesirable area. This practically results in sample rates faster than 1.0 Hz being necessary. Furthermore, interpolation will be required in the costmap to inflate FMCW observations into the configuration space of the robot. However, the fluctuations seen in dynamic testing in either RSA may become spatially averaged out, effectively masking the clear difference seen in the static tests. The consequence of this may be that a robot is unable to reliably distinguish between dry areas and those with only a small amount of moisture when in motion. Despite this, FMCW demonstrates itself as a strong candidate method to provide autonomous robotic systems with awareness of surface and subsurface ground integrity candidate method to provide autonomous robotic systems with awareness of surface and subsurface ground integrity.

VI. CONCLUSION

The provision of autonomous path planning and run-time evasive action decision-making, in the event of an identified terrain hazard, has significant cross-sector and cross-application potential. The FMCW sensing modality has been shown to be effective for the detection of surface water and integration with a UGV has demonstrated that this novel application of millimeter wave sensing has the potential to add to full-field non-contact sensing capabilities in SLAM for RAS and provides a clear advantage over currently applied systems to assess for surface water, *in situ*, by a deployed RAS while not requiring direct contact with the surface being evaluated.

The future incorporation of robotically deployed FMCW sensitivity to these measurands will lead to enhanced situational awareness, improving the ability of field robots to operate in the dynamic and harsh environments of unmanaged sites with minimal human intervention. To achieve this, this research aims to evaluate the FMCW sensing modality on wheeled and quadruped robots operating in areas where human presence is denied. Further work will include the fusion of the FMCW modality with other non-standard environmental sensors, such as alpha and gamma radiation detectors fitted to Continuous Autonomous Radiation Monitoring Assistant (CARMA), a Clearpath Jackal heavily modified for operations within nuclear environments [6], [7]. The CARMA platform has been designed to operate in areas that have been sealed off from human presence due to significant radiation risks and has a

suite of radiation detectors on board to map areas of interest. The data acquired from CARMA is transmitted to a base station and overlain on a LiDAR map of the area. The integration of the FMCW with this sensor suite will allow the human-in-the-loop to interrogate a region of detected radiation to determine if the source is a fluid, allowing for autonomous tracking to the source of the radiation leak.

Future work will further develop the FMCW application to ground integrity monitoring for additional factors in robotic warehouse operations, such as oil spillage and sensor angle of incidence variation to provide improved forward visibility of the planned path. Future work will also investigate uneven and unprepared terrain, such as loose sand or deep snow. Additions to the software will allow the robot to make decisions regarding safe path planning and mission feasibility based on this additional information stream, while improvements to the sensor data acquisition rate will enhance the spatial resolution of datasets and resultant mapping.

ACKNOWLEDGMENTS

IMPORTANT: All regular papers go through a blind peer-review process. Therefore, your submission must not include information that serves to identify the authors of the manuscript, such as name(s) or affiliation(s) of the author(s), anywhere in the manuscript, abstract, or in the embedded PDF data. References and bibliographic citations to the author(s) own published works or affiliations should be made in the third person.

REFERENCES

- [1] K. Azadeh, R. de Koster, and D. Roy, "Robotized Warehouse Systems: Developments and Research Opportunities," *ERIM report series research in management Erasmus Research Institute of Management*, May 2017.
- [2] M. S. Ganeshmurthy and G. R. Suresh, "Path planning algorithm for autonomous mobile robot in dynamic environment," *2015 3rd International Conference on Signal Processing, Communication and Networking, ICSCN 2015*, Aug. 2015, doi: 10.1109/ICSCN.2015.7219901.
- [3] M. Zaffar, S. Ehsan, R. Stolkin, and K. M. D. Maier, "Sensors, SLAM and Long-term Autonomy: A Review," *2018 NASA/ESA Conference on Adaptive Hardware and Systems, AHS 2018*, pp. 285–290, Nov. 2018, doi: 10.1109/AHS.2018.8541483.
- [4] A. West *et al.*, "Use of Gaussian process regression for radiation mapping of a nuclear reactor with a mobile robot," *Scientific Reports 2021 11:1*, vol. 11, no. 1, pp. 1–11, Jul. 2021, doi: 10.1038/s41598-021-93474-4.
- [5] D. v. Lu, D. Hershberger, and W. D. Smart, "Layered costmaps for context-sensitive navigation," *IEEE International Conference on Intelligent Robots and Systems*, pp. 709–715, Oct. 2014, doi: 10.1109/IROS.2014.6942636.
- [6] A. West, T. Wright, I. Tsitsimpelis, K. Groves, M. J. Joyce, and B. Lennox, "Real-Time Avoidance of Ionising Radiation Using Layered Costmaps for Mobile Robots," *Front Robot AI*, vol. 9, pp. 1–13, Mar. 2022, doi: 10.3389/frobt.2022.862067.
- [7] K. Groves, E. Hernandez, A. West, T. Wright, and B. Lennox, "Robotic Exploration of an Unknown Nuclear Environment Using Radiation Informed Autonomous Navigation," *Robotics 2021, Vol. 10, Page 78*, vol. 10, no. 2, p. 78, May 2021, doi: 10.3390/ROBOTICS10020078.
- [8] Y. Xu *et al.*, "A Flexible Multimodal Sole Sensor for Legged Robot Sensing Complex Ground Information during Locomotion," *Sensors 2021, Vol. 21, Page 5359*, vol. 21, no. 16, p. 5359, Aug. 2021, doi: 10.3390/S21165359.
- [9] J. H. Kim, "Multi-Axis Force-Torque Sensors for Measuring Zero-Moment Point in Humanoid Robots: A Review," *IEEE Sens J*, vol. 20, no. 3, pp. 1126–1141, Feb. 2020, doi: 10.1109/JSEN.2019.2947719.
- [10] D. Wisth, M. Camurri, and M. Fallon, "Robust Legged Robot State Estimation Using Factor Graph Optimization," *IEEE Robot Autom Lett*, vol. 4, no. 4, pp. 4507–4514, Oct. 2019, doi: 10.1109/LRA.2019.2933768.
- [11] L. Lynch, T. Neue, J. Clifford, J. Coleman, J. Walsh, and D. Toal, "Automated Ground Vehicle (AGV) and sensor technologies-A review," *Proceedings of the International Conference on Sensing Technology, ICST*, vol. 2018-December, pp. 347–352, Jan. 2019, doi: 10.1109/ICSENST.2018.8603640.
- [12] F. Jenelten, J. Hwangbo, F. Tresoldi, C. D. Bellicoso, and M. Hutter, "Dynamic Locomotion on Slippery Ground," *IEEE Robot Autom Lett*, vol. 4, no. 4, pp. 4170–4176, Jul. 2019, doi: 10.1109/LRA.2019.2931284.
- [13] R. Bogue, "Growth in e-commerce boosts innovation in the warehouse robot market," *Industrial Robot*, vol. 43, no. 6, pp. 583–587, 2016, doi: 10.1108/IR-07-2016-0194/FULL/PDF.
- [14] D. Vivet, P. Checchin, and R. Chapuis, "Localization and mapping using only a rotating FMCW radar sensor," *Sensors (Switzerland)*, vol. 13, no. 4, pp. 4527–4552, Apr. 2013, doi: 10.3390/s130404527.
- [15] D. Vivet, P. Checchin, R. Chapuis, P. Faure, R. Rouveure, and M. O. Monod, "A mobile ground-based radar sensor for detection and tracking of moving objects," *EURASIP J Adv Signal Process*, vol. 2012, no. 1, pp. 1–13, Feb. 2012, doi: 10.1186/1687-6180-2012-45/FIGURES/19.
- [16] E. Miralles *et al.*, "Multifunctional and compact 3D FMCW MIMO radar system with rectangular array for medium-range applications," *IEEE Aerospace and Electronic Systems Magazine*, vol. 33, no. 4, pp. 46–54, Apr. 2018, doi: 10.1109/MAES.2018.160277.
- [17] N. Wessendorp, R. Dinaux, J. Dupeyroux, and G. C. H. E. de Croon, "Obstacle Avoidance onboard MAVs using a FMCW Radar," *IEEE International Conference on Intelligent Robots and Systems*, pp. 117–122, 2021, doi: 10.1109/IROS51168.2021.9635901.
- [18] P. Nimac, T. Petrič, A. Krpič, and A. Gams, "Evaluation of FMCW Radar for Potential Use in SSM," *Mechanisms and Machine Science*, vol. 120 MMS, pp. 580–588, 2022, doi: 10.1007/978-3-031-04870-8_68/FIGURES/3.
- [19] S. Edstaller and D. Mueller, "A Human-Machine Distance Control System Using Incoherent Cooperative FMCW Radar Sensors," *2021 18th European Radar Conference, EuRAD 2021*, pp. 1–4, 2021, doi: 10.23919/EURAD50154.2022.9784549.
- [20] H. P. Marshall, M. Schneebeli, and G. Koh, "Snow stratigraphy measurements with high-frequency FMCW radar: Comparison with snow micro-penetrometer," *Cold Reg Sci Technol*, vol. 47, no. 1–2, pp. 108–117, Jan. 2007, doi: 10.1016/J.COLDREGIONS.2006.08.008.
- [21] G. Koh, J. H. Lever, S. A. Arcone, H. P. Marshall, and L. E. Ray, "Autonomous FMCW radar survey of Antarctic shear zone," in *13th International Conference on Ground Penetrating Radar*, Aug. 2010, doi: 10.1109/ICGPR.2010.5550174.
- [22] H. P. Marshall and G. Koh, "FMCW radars for snow research," *Cold Reg Sci Technol*, vol. 52, no. 2, pp. 118–131, Apr. 2008, doi: 10.1016/J.COLDREGIONS.2007.04.008.
- [23] N. Galin *et al.*, "2–8 GHz FMCW radar for estimating snow depth on antarctic sea ice," in *International Conference on Radar*, Oct. 2008, pp. 276–281, doi: 10.1109/RADAR.2008.4653931.
- [24] N. Galin, A. Worby, T. Markus, C. Leuschen, and P. Gogineni, "Validation of airborne FMCW radar measurements of snow thickness over sea ice in antarctica," *IEEE Transactions on Geoscience and Remote Sensing*, vol. 50, no. 1, pp. 3–12, Jan. 2012, doi: 10.1109/TGRS.2011.2159121.
- [25] J. H. Bradford, H. Marshall, J. H. Bradford, and H. Marshall, "Estimating complex dielectric permittivity of soils from spectral ratio analysis of swept frequency (FMCW) ground-penetrating radar data (Invited)," *American Geophysical Union, Fall Meeting*,

- vol. 2010, pp. H21K-06, 2010, Accessed: Jan. 18, 2022. [Online]. Available: <https://ui.adsabs.harvard.edu/abs/2010AGUFM.H21K..06B/abstr.act>
- [26] R. A. Taylor *et al.*, "A Prototype Ultra-Wideband FMCW Radar for Snow and Soil-Moisture Measurements," *International Geoscience and Remote Sensing Symposium (IGARSS)*, pp. 3974–3977, Jul. 2019, doi: 10.1109/IGARSS.2019.8899024.
- [27] D. Mitchell, J. Blanche, and D. Flynn, "An Evaluation of Millimeter-wave Radar Sensing for Civil Infrastructure," *11th Annual IEEE Information Technology, Electronics and Mobile Communication Conference, IEMCON 2020*, pp. 216–222, Nov. 2020, doi: 10.1109/IEMCON51383.2020.9284883.
- [28] J. Blanche, J. Buckman, H. Lewis, and D. Flynn, "Frequency modulated continuous wave analysis of dynamic load deformation in geomaterials," in *Offshore Technology Conference*, May 2020. doi: 10.4043/30479-ms.
- [29] K. van Loon *et al.*, "Wireless non-invasive continuous respiratory monitoring with FMCW radar: a clinical validation study," *J Clin Monit Comput*, vol. 30, no. 6, pp. 797–805, Dec. 2016, doi: 10.1007/S10877-015-9777-5/FIGURES/5.
- [30] P. Jena and K. N. Sahu, "Millimeter Wave FMCW Radar for contactless diagnosis of cardiovascular diseases," *2nd International Conference on Range Technology, ICORT 2021*, Aug. 2021, doi: 10.1109/ICORT52730.2021.9582031.
- [31] Y.-C. Shen *et al.*, "The signal processing algorithm of automotive FMCW radars with an extended range of speed estimation," *J Phys Conf Ser*, vol. 1236, no. 1, p. 012081, Jun. 2019, doi: 10.1088/1742-6596/1236/1/012081.
- [32] R. Wan, Y. Song, T. Mu, and Z. Wang, "Moving target detection using the 2D-FFT algorithm for automotive FMCW radars," *Proceedings - 2019 International Conference on Communications, Information System, and Computer Engineering, CISCE 2019*, pp. 239–243, Jul. 2019, doi: 10.1109/CISCE.2019.00062.
- [33] W. Kim, H. Cho, J. Kim, B. Kim, and S. Lee, "YOLO-Based Simultaneous Target Detection and Classification in Automotive FMCW Radar Systems," *Sensors 2020, Vol. 20, Page 2897*, vol. 20, no. 10, p. 2897, May 2020, doi: 10.3390/S20102897.
- [34] F. Hau, F. Baumgärtner, and M. Vossiek, "The degradation of automotive radar sensor signals caused by vehicle vibrations and other nonlinear movements," *Sensors (Switzerland)*, vol. 20, no. 21, pp. 1–17, Nov. 2020, doi: 10.3390/s20216195.
- [35] S. Lee, J. Y. Lee, and S. C. Kim, "Mutual Interference Suppression Using Wavelet Denoising in Automotive FMCW Radar Systems," *IEEE Transactions on Intelligent Transportation Systems*, vol. 22, no. 2, pp. 887–897, Feb. 2021, doi: 10.1109/TITS.2019.2961235.
- [36] K. Siddiq, M. K. Hobden, S. R. Pennock, and R. J. Watson, "Phase noise in FMCW radar systems," *IEEE Trans Aerosp Electron Syst*, vol. 55, no. 1, pp. 70–81, Feb. 2019, doi: 10.1109/TAES.2018.2847999.
- [37] G. Beziuk, T. C. Baum, K. Ghorbani, and K. J. Nicholson, "Structurally Integrated Radar in an Aerospace Composite Laminate," *IEEE Trans Compon Packaging Manuf Technol*, vol. 11, no. 11, pp. 1835–1843, Nov. 2021, doi: 10.1109/TCPMT.2021.3118108.
- [38] P. R. Midhunkrishna, M. J. Lal, S. Joy, K. K. Mukundan, and M. Nambhootheripad, "Design & implementation of algorithm for linear sweep generation and signal processing for an FMCW radar altimeter," *2021 8th International Conference on Smart Computing and Communications: Artificial Intelligence, AI Driven Applications for a Smart World, ICSCC 2021*, pp. 140–144, Jul. 2021, doi: 10.1109/ICSCC51209.2021.9528231.
- [39] W. Zhang, H. Li, G. Sun, and Z. He, "Enhanced Detection of Doppler-Spread Targets for FMCW Radar," *IEEE Trans Aerosp Electron Syst*, vol. 55, no. 4, pp. 2066–2078, Jul. 2019, doi: 10.1109/TAES.2019.2925433.
- [40] M. E. Yanik and M. Torlak, "Near-Field 2-D SAR imaging by millimeter-wave radar for concealed item detection," *IEEE Radio and Wireless Symposium, RWS*, May 2019, doi: 10.1109/RWS.2019.8714552.
- [41] A. Rizik, E. Tavanti, H. Chible, D. D. Caviglia, and A. Randazzo, "Cost-Efficient FMCW Radar for Multi-Target Classification in Security Gate Monitoring," *IEEE Sens J*, vol. 21, no. 18, pp. 20447–20461, Sep. 2021, doi: 10.1109/JSEN.2021.3095674.
- [42] W. Tang, D. Mitchell, J. Blanche, R. Gupta, and D. Flynn, "Machine Learning Analysis of Non-Destructive Evaluation Data from Radar Inspection of Wind Turbine Blades," in *International Conference on Sensing, Diagnostics, Prognostics, and Control (SDPC)*, Oct. 2021, pp. 122–128. doi: 10.1109/sdpc52933.2021.9563264.
- [43] L. Maio *et al.*, "Detection of ice accretions on composite panels using FMCW radars at 60GHz," *2021 IEEE International Workshop on Metrology for AeroSpace, MetroAeroSpace 2021 - Proceedings*, pp. 636–639, Jun. 2021, doi: 10.1109/METROAEROSPACE51421.2021.9511775.
- [44] C. Cadena *et al.*, "Past, present, and future of simultaneous localization and mapping: Toward the robust-perception age," *IEEE Transactions on Robotics*, vol. 32, no. 6, pp. 1309–1332, Dec. 2016, doi: 10.1109/TRO.2016.2624754.
- [45] J. Blanche *et al.*, "Dynamic Fluid Ingress Detection in Geomaterials Using K-Band Frequency Modulated Continuous Wave Radar," *IEEE Access*, vol. 8, pp. 111027–111041, 2020, doi: 10.1109/ACCESS.2020.3002147.
- [46] W. J. Duffin, *Electricity and Magnetism*, 4th ed. Maidenhead: McGraw-Hill, 1990.
- [47] J. G. D. Oliveira, J. G. D. Junior, E. N. M. G. Pinto, V. P. S. Neto, and A. G. D'Assunção, "A New Planar Microwave Sensor for Building Materials Complex Permittivity Characterization," *Sensors 2020, Vol. 20, Page 6328*, vol. 20, no. 21, p. 6328, Nov. 2020, doi: 10.3390/S20216328.
- [48] H. Zadhoush, A. Giannopoulos, and I. Giannakis, "Optimising the Complex Refractive Index Model for Estimating the Permittivity of Heterogeneous Concrete Models," *Remote Sensing 2021, Vol. 13, Page 723*, vol. 13, no. 4, p. 723, Feb. 2021, doi: 10.3390/RS13040723.
- [49] Jurgen H. Schon, "Physical Properties of Rocks: A Workbook," *Handbook of Petroleum Exploration and Production*, vol. 8, pp. 345–348, 2011.
- [50] J. Blanche, D. Mitchell, R. Gupta, A. Tang, and D. Flynn, "Asset Integrity Monitoring of Wind Turbine Blades with Non-Destructive Radar Sensing," *11th Annual IEEE Information Technology, Electronics and Mobile Communication Conference, IEMCON 2020*, pp. 498–504, Nov. 2020, doi: 10.1109/IEMCON51383.2020.9284941.
- [51] J. Blanche *et al.*, "Dynamic Fluid Ingress Detection in Geomaterials Using K-Band Frequency Modulated Continuous Wave Radar," *IEEE Access*, vol. 8, pp. 111027–111041, 2020, doi: 10.1109/ACCESS.2020.3002147.